ELSEVIER

Materials Science and Engineering A 435–436 (2006) 504–514

MATERIALS SCIENCE & ENGINEERING A

www.elsevier.com/locate/msea

Interaction of hydrogen with the microstructure of low-carbon steel

V.P. Ramunni [a,b,*], T. De Paiva Coelho [c], P.E.V. de Miranda [d]

[a] *Departamento de Materiales, CAC/CNEA, Av. General Paz 1499, CP 1650 San Martín, Prov. de Buenos Aires, Argentina*
[b] *CONICET, Av. Rivadavia 1917, C1033AAJ Buenos Aires, Argentina*
[c] *CEFETES, Av. Vitória 1729, 291101-040 Jucutucuara, Vitória, ES, Brazil*
[d] *Metallurgical and Materials Engineering Department, Federal University of Rio de Janeiro, CP 68.505, CEP21945 Rio de Janeiro, Brazil*

Received 7 March 2006; received in revised form 10 July 2006; accepted 21 July 2006

Abstract

The interaction of hydrogen (H) with the microstructure of SAE 1008 type low-carbon steel is studied in this work. The objective is to determine the binding energy, ΔE, of H with the cementite (Fe_3C) for three different conditions of the carbide. Electrochemical permeation tests are combined with the numerical resolution of Fick's equations assuming that hydrogen is delayed during de transport by reversible trapping sites. Techniques of H vacuum desorption are also employed to describe irreversible trapping. From permeation tests, we obtain the density of reversible trapping sites and the probabilities of H capture and release from which ΔE is evaluated. From effusion test, weak and strong trapping sites with energies in the range of $\Delta E \approx 10$–50 kJ/mol H were observed.
© 2006 Published by Elsevier B.V.

Keywords: Low-carbon steels; Hydrogen embrittlement; Electrochemical permeation; Vacuum desorption technique; Trapping sites; Binding energy

1. Introduction

It is known that microstructural alterations induced by thermal treatments modify the kinetic of hydrogen diffusion, qualitatively demonstrated by Bott et al. for low-carbon steels [1]. Alterations in permeation parameters are observed when H in solution is present and some doubts must be entertained about the validity of Fick's laws and their associated physical model of non-interacting particles in random motion through the medium. The presence of hydrogen (H) in solid solution in metals and alloys is related mainly to the small diameter of this element and its capacity to diffuse with certain ease in solid state. Different factors contribute to elevate or diminish the solubilization and/or diffusion of H in steels. The main ones are temperature, alloy composition, crystalline structure and substructure. Nevertheless, the presence of H in metals and specifically in steels is not desired in most of the cases, since H alters considerably the mechanical–metallurgic properties of these materials with the possibility of fracture. The most typical damage caused by H in steel is embrittlement. Embrittlement due to H involves a vast loss of mechanical properties with the following characteristics such as, for example, decrease of ductility and fracture tension with the increase of H concentration. There are changes in the type of fractures from a typically ductile morphology to one essentially fragile. Embrittlement occurs mainly on the interval of temperatures between -100 and $100\,^{\circ}C$, with the maximum effect at room temperature.

The steel studied in the present work has been designed to obtain a high deformability, ductility and surface quality at a low cost. The select microstructures for the present study are: pro-eutectoid ferrite + fine pearlite (P), a spheroidized structure containing ferrite + fine globular cementite (G) and an aged (A) structure containing very fine carbide particles in a ferritic matrix. Previous experimental evidences [1] have motivated the present work and we pretend to determine the degree of reversibility of the three morphologies of the cementite recognized as trapping sites at $T = 27\,^{\circ}C$.

The methodology employed in this work is based on the mathematical model developed by McNabb and Foster [2] to reformulate Fick's second law in the presence of trapping sites. We solve the system of coupled differential equations using IMSL [3] subroutines and within our picture we reproduce the Ferris' procedure [4] to relate all diffusion parameters to the experimental permeation curves in terms of the constants of the trapping theory. The "differential thermal analysis" methodology adapted by Choo and Lee [5] is employed

* Corresponding author.
E-mail address: vpram@cnea.gov.ar (V.P. Ramunni).

0921-5093/$ – see front matter © 2006 Published by Elsevier B.V.
doi:10.1016/j.msea.2006.07.089

to calculate the binding energy from vacuum desorption tests.

A sheet of low-carbon steel is submitted to a scheme of heat treatments to obtain the three morphologies of the cementite under study. The inspection of these structures of the carbide is based on superficial observation employing transmission electron and optical microscopy. The objective of the present work is to make the treatment based on the local equilibrium hypothesis more specific, in order to show how relevant parameters can be evaluated from experiments. The interrelated parameters that quantify the permeation behavior characteristics of the material: the apparent diffusivity D_{app} and the apparent solubility S_{app}, where S_{app} means the total hydrogen content in solid solution and occluded in traps, are also explored here. These results give us some information concerning the nature of the trapping site in low-carbon steels.

Therefore, metallographic, electrochemical and vacuum techniques as well as numerical calculation analysis are combined to study the behavior of hydrogen diffusion through a low-carbon steel matrix. Following the procedure of Ferris and Turnbull [4] the relevant parameters that characterize the diffusion process in presence of reversible trapping sites are explained. We obtain an expression for the binding energy ΔE, related to the permeation tests parameters, from a model developed by Oriani [6] associated to the trapping site. In order to investigate irreversible trapping sites by thermal analysis, vacuum desorption is performed on samples previously submitted to electrochemical H charging.

We obtain from electrochemical techniques $|\Delta E| \leq k_B T$ indicating that the three morphologies of the cementite are reversible traps (weak) of H at room temperature consistently with experimental values of apparent solubility obtained by Bott et al. [1]. From effusion tests, the presence of effusion peaks of H are observed at typical temperatures, originating in the selective desorption together with the cementite and other microstructural species present in the samples. It is also observed that, with the variation of the heating rate applied to the samples during the effusion tests, temperatures where peaks occur are changed. These results allow to establish a correspondence of the effusion peaks of H with the cementite and dislocations acting as distinct trapping sites. The values of binding energies found with this technique are: 13.07 ± 1.59 kJ/mol H and 12.89 ± 3.42 kJ/mol H for the incoherent interphases of the cementite and the ferritic matrix of the respectively, spheroidized and normalized samples. While the energies found for dislocations are 27.78 ± 3.57 kJ/mol H for the spheroidized samples and 25.41 ± 3.07 kJ/mol H for the normalized ones. Due to the microstructural instability of the aged sample, it is not possible to determine, in this case, the corresponding binding energy.

In Section 2, we briefly describe the modified Fick's equations in presence of reversible traps proposed by McNabb and Foster [2]. The relation between the model herein adopted the electrochemical permeation curves is explained in Section 3 to obtain an expression of the binding energy ΔE. The experimental procedure for the electrochemical permeation tests and the vacuum H desorption techniques, together with a flowchart of heat treatments to obtain the microstructures under study are described in Section 4. Finally, an analysis of the results and the methodology adopted in the present work is discussed.

2. Mathematical formulation: the model

In accordance to Fick's second law, the concentration of diffusing H atoms (interstitial plus trapped), $C(x, t)$, at time t satisfies:

$$\frac{\partial C(x,t)}{\partial t} = D_L \frac{\partial^2 C(s,t)}{\partial x^2}, \tag{1}$$

where D_L is the diffusion constant. From Fick's first law, the flux of hydrogen flowing through an arbitrary surface S in the metal is

$$\int_S D_L \vec{\nabla} C(x,t) \hat{n}\, \mathrm{d}S, \tag{2}$$

where $\hat{n}$ is a unit vector normal to the surface S. In addition, we suppose that the metal contains a uniformly distributed population of "traps" with different capacities of capturing and delaying hydrogen atoms. According to the strength with which they hold captured atoms the traps are classified, at the steady state, as

- *Reversible*: when the amount of trapped hydrogen is in equilibrium with that in diffusion process, or
- *Irreversible*: when it has a concentration of hydrogen atoms that is independent of the diffusing through the metal. H in irreversible traps is permanently removed from the diffusion process over time intervals and at the considered temperatures.

N_r is the density of reversible traps and n_r the fraction of these, occupied by hydrogen atoms. The traps can be described in their overall effect by two parameters, p_r and k_r, which represent the average probability that a hydrogen atom be respectively released or captured for a reversible trap before a second had passed. It is postulated that these probabilities depends on the temperature and on the nature of the trap but do not depend on the local concentration of trapped and diffusing hydrogen. In this way, the number of liberated atoms per second in a volume δV is proportional to the number of occupied traps and therefore given by,

$$p_r n_r N_r \delta V, \tag{3}$$

and the number of liberated atoms per second in δV is

$$k_r C(x,t) N_r (1 - n_r) \delta V, \tag{4}$$

which is proportional to the concentration of diffusing atoms $C(x, t)$ and to $N_r(1 - n_r)$ the number of vacant traps per unit volume. Considering the flux of hydrogen atoms $Q(t)$ in V at time t is

$$Q(t) = \int_V (C(x,t) + n_r N_r)\, \mathrm{d}V, \tag{5}$$

and let be the flux of hydrogen atoms through the bounding surface S of V of an isotropic homogeneous medium containing

N_r reversible traps per unit volume:

$$\frac{\partial Q(t)}{\partial t} = \int_S D_L \vec{\nabla} C(x,t)\hat{n}\,dS, \tag{6}$$

time differentiating $Q(t)$ from Eq. (5):

$$\frac{\partial Q(t)}{\partial t} = \int_V \left(\frac{\partial C(x,t)}{\partial t} + N_r \frac{\partial n_r}{\partial t} \right) dV, \tag{7}$$

is obtained. Equating Eqs. (6) and (7), using the divergence theorem, and assuming that D_L is independent of the concentration and the position, the equation of continuity for $C(x, t)$ is

$$\frac{\partial C(x,t)}{\partial t} + N_r \frac{\partial n_r}{\partial t} = D_L \vec{\nabla}^2 C(x,t), \tag{8}$$

It is assumed that irreversible traps are saturated and do not have influence on the diffusion process. A second equation involving $n_r(x, t)$ and $C(x, t)$ is obtained by considering the rate of interchange of hydrogen atoms between the trapped and diffusing populations.

$$\frac{\partial n_r}{\partial t} = k_r C(x,t)(1 - n_r) - p_r n_r, \tag{9}$$

which expresses that the variation of the concentration of atoms diffusing in the lattice depends on the loss of hydrogen atoms in the traps and on the gain of hydrogen atoms from them. Eqs. (8) and (9) describe the kinetic of hydrogen diffusion through an isotropic homogeneous medium containing a uniformly distributed reversible population of traps. To solve the coupled system of equations it is necessary to establish appropriate boundary conditions. Considering a plate of metal initially free of hydrogen, if the concentration of diffusing hydrogen is maintained at C_0 on the face $x = a$ (or $\chi = x/a = 1$) and zero on the other, the flux through this second face will be zero initially but gradually increase to a constant value $C_0 D_L/a$,

$$\begin{cases} t = 0, & C = 0,\ 0 \le x \le a, \\ t > 0 & \begin{cases} C = C_0, & x = 0, \\ C = 0, & x = a, \end{cases} \end{cases} \tag{10}$$

C_0 is the hydrogen solubility at the sample surface. For these conditions, the exact solution to the necessary time to reach the steady state is given by [4]:

$$t = \frac{a^2}{D_L}\left[\frac{1}{6} + \frac{\alpha}{2\beta} + \frac{\alpha}{\beta^2} + \frac{\alpha}{\beta^3}(1+\beta)\ln(1+\beta)\right], \tag{11}$$

where $\alpha = N_r k_r/p_r$ and $\beta = C_0 k_r/p_r$. It is useful to express Eqs. (8)–(10) in a dimensionless form. In order to do this, we define $\tau = D_L t/a^2$, $\chi = x/a$, $u = C/C_0$, $v = N_r n_r/C_0$, $\lambda = N_r k_r a^2/D_L$, $\mu = p_r a^2/D_L$ and $\rho = C_0/N_r$, where a is a representative length such as the thickness of the specimen. Performing the transformation $(x, t) \to (\chi, \tau)$, Eqs. (8) and (9) and the boundary conditions (10) become:

$$\frac{\partial u}{\partial \tau} = \frac{\partial^2 u}{\partial \chi^2} - \lambda u(1 - \rho v) + \mu v, \tag{12}$$

$$\frac{\partial v}{\partial \tau} = \lambda u(1 - \rho v) - \mu v, \tag{13}$$

and

$$\begin{cases} \tau = 0, & u = v = 0, \\ \tau > 0 & \begin{cases} u = 1, & \chi = 0, \\ u = 0, & \chi = 1, \end{cases} \end{cases} \tag{14}$$

λ, μ and ρ, including D_L, are relevant parameters that describe the kinetic of H diffusion in presence of trapping in steels. For computing the binding energy, a specific model for the trapping site is necessary, which is described in the next section.

3. Expression for the binding energy ΔE

The reversibility is associated to the intensity with which a trapping site or "trap" retains the hydrogen atoms diffusing in the lattice. In terms of activation energies, Oriani [6] developed a model in which a trapping site is regarded as a potential well of significantly greater depth (ΔE) than those encountered in regular regions of the crystal lattice. Referring to Fig. 1, the trapping site represents an energy level lower than that of a normal site by ΔE, and it is bounded by an energy barrier of height $E' + E_a$, where E_a is the activation energy for jumping between normal lattice sites separated by the distance λ. Relating E_a, E' and ΔE and neglecting the entropy factors, the rate of escape p_r and capture k_r per trap may be expressed as

$$p_r = \sigma_0 \exp\left[\frac{\Delta E - (E_a + E')}{RT}\right], \tag{16}$$

$$k_r = \sigma_0 \exp\left[-\frac{(E_a + E')}{RT}\right], \tag{17}$$

respectively, in which σ_0 is the vibrational frequency of the trapped hydrogen, taken the same as that of hydrogen on normal lattice sites, T is the absolute temperature expressed in K and R the ideal constant gases. From Eqs. (16) and (17), we express the equilibrium constant between two atomics population, the diffusing and the trapped ones, as a function of ΔE:

$$\kappa = \frac{k_r}{p_r} = \exp\left(-\frac{\Delta E}{RT}\right). \tag{18}$$

It is possible to relate the equilibrium constant κ, with the dimensionless λ, μ and ρ to obtain an expression for ΔE. This procedure connects the experimental electrochemical curves with the theoretical model for reversible traps as described below.

The equilibrium between the two atomic populations, each one occupying a fraction n_i of available sites can be described

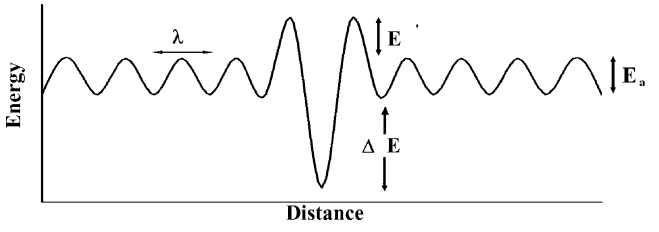

Fig. 1. Model for trapping site.

from the equilibrium constant κ usually expressed as

$$C_L + C_x \leftrightarrow C_r, \tag{19}$$

where C_L is the hydrogen atoms concentration dissolved in the lattice, C_x the trap concentration and C_r the trapped hydrogen concentration. Then, the equilibrium constant κ expressed as a function of the hydrogen activities a_L and a_r corresponding to normal and trapping sites respectively, can be written as

$$\kappa = \frac{a_r}{a_L}, \tag{20}$$

If it is assumed that both kinds of sites constitute finite populations and do not interact between them, the activities can be written as a function of the available sites n_i according to,

$$a_i = \frac{n_i}{1 - n_i}, \tag{21}$$

assuming that $C_L = n_L N_L$, $n_L \ll 1$, where N_L which depends on the lattice structure is the density of normal sites assumed given and n_L is the fraction of normal sites occupied by hydrogen atoms. κ is expressed as [6]:

$$\kappa = \frac{1}{n_L}\left(\frac{n_r}{1 - n_r}\right), \tag{22}$$

If the equilibrium is established when the sample is charged with hydrogen at a determined temperature T from Eq. (9), $\partial n_r/\partial t = 0 = k_r C_L(1 - n_r) - p_r n_r$, being $C_L = n_L N_L$ and from Eq. (22) we obtain:

$$N_L \frac{k_r}{p_r} = \frac{n_r}{n_L(1 - n_r)} = \kappa. \tag{23}$$

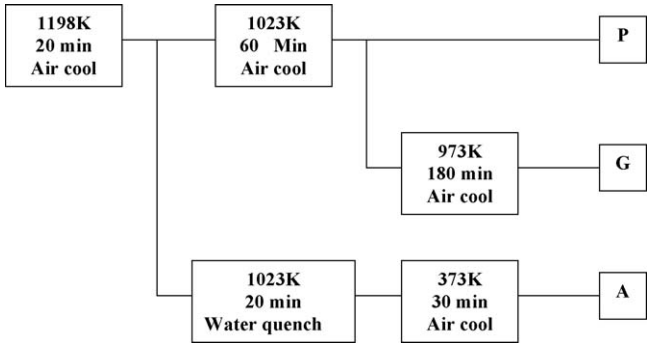

Fig. 2. Scheme of heat treatment.

Rewriting the left term in Eq. (23) as a function of the dimensionless $\lambda = N_r a^2 k_r/D_L$, $\mu = a^2 p_r/D_L$ and $\rho = C_0/N_r$, the expression for ΔE is obtained in terms of the parameters related to reversible traps:

$$N_L \frac{k_r}{p_r} = \frac{N_L}{C_0}\rho\left(\frac{\lambda}{\mu}\right) = \exp\left(-\frac{\Delta E}{RT}\right). \tag{24}$$

The best estimative of this parameter is obtained from martensitic steels, i.e., $N_L = 2.6 \times 10^{23}$ sites/cm^3 corresponding to octahedric sites and $N_L = 5.2 \times 10^{23}$ sites/cm^3 for tetrahedric sites.

4. Experimental techniques

4.1. Materials and methods

A SAE 1008 low-carbon steel plate, with chemical composition (wt.%): C 0.08, Mn 0.31, Si <0.001, S 0.0021, Ti >0.01,

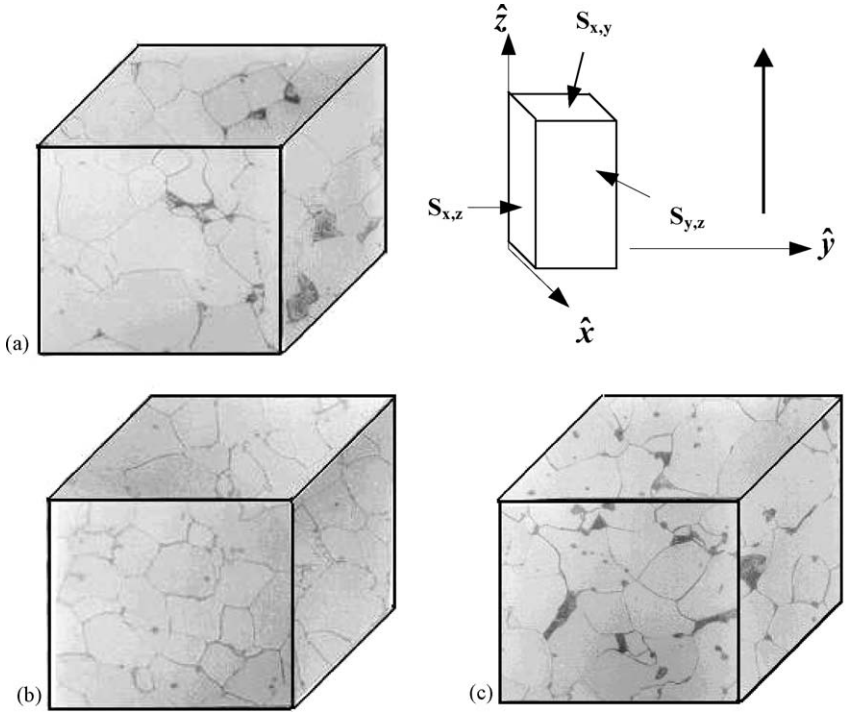

Fig. 3. Optical microscopy results: (a) aged sample A; (b) globular condition, G; (c) pearlitic condition, P. Zoom 510×. Optical microscopy shows a constant ferrite grain size of for the three conditions of the carbide.

P 0.005, and Al 0.02 is employed. This steel has been developed aiming to obtaining a high deformability, ductility and surface quality at low cost. Sheets of 1.0 mm average thickness are subjected to a procedure of heat treatments described in Fig. 2 [1]. The resulting microstructures are pro-eutectoid ferrite + fine pearlite (P), a spheroidized structure containing ferrite + fine globular cementite (G), and an aged (A) structure containing very fine carbide particles in a ferritic matrix. The samples are then cut and polished with 1 μ diamond paste, and observed by optical microscopy (OM) and transmission electron microscopy (TEM). The TEM and OM results for the carbides are shown in Figs. 3 and 4, respectively; OM results show a uniform ferrite grain size for the three microstructures.

4.2. Electrochemical permeation tests

A two-compartment electrochemical permeation cell developed by Bott et al. [1] is used. The tests are performed by real-time computer monitoring and data analysis *via* a programmable multichannel control unit. Both compartments of the electrochemical cell are filled with 0.1 M NaOH, and continuous nitrogen bubbling is maintained throughout the test. H is generated cathodically at the sample surface in one of the compartments, employing a constant potential of −1.35 V with respect to a saturated calomel electrode (SCE), and detected by anodic polarization at the corrosion potential in the adjacent compartment, after permeating through the thin metallic sheet separating the two (WE). The main components of the detection cell are shown in Fig. 5. The progress of the H permeation process is followed by monitoring the evolution of the anodic current (I_a), measured between the specimen and the counter electrode (CE) of the detection compartment. A temperature of (27 ± 1) °C is maintained throughout the test using silicon transistor sensor. A thin layer of Pd is deposited on the sample surface exposed to the H generation compartment. The solubility of H in Pd is greater than in steel, so that a considerable H concentration gradient to start the diffusion test is generated.

4.3. Thermal effusion tests in vacuum

H effusion tests in vacuum measure the elimination of the H contained in a previously hydrogenated sample, as a function of temperature. Consequently, the H in the sample, which does not diffuse at room temperature since it is trapped in "traps", is liberated at a given heating rate imposed by the experimental conditions. The equipment is made out of a reaction tube, a mobile furnace, a high vacuum turbomolecular pump, and a controlling computer. The results of this test determine the binding energy, ΔE, of H with the traps present in the studied sample. All samples destined to effusion tests are previously hydrogenated during an hour of cathodical charge in an electrolytic solution of NaOH 0.1N, at a temperature of (27.0 ± 0.1) °C thermostatized by water circulation. The current necessary for hydrogenation is obtained by analyzing the polarization curves. Temperature, time, and hydrogenation profile are monitored during the test. After hydrogenation, samples are stored in liquid nitrogen for an average time of 12 h. Reversible and irreversible trapping sites

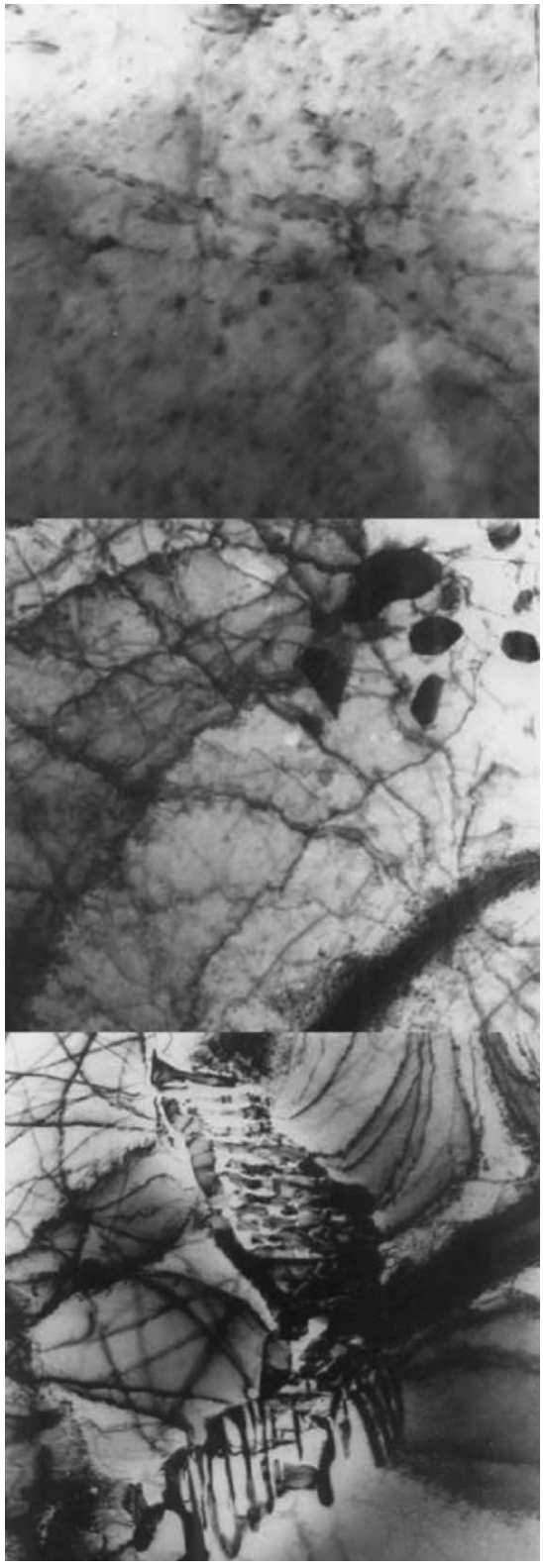

Fig. 4. Transmission electron micrography. (Top) The aged condition, A. Carbide morphology: very fine intergranular cementite. (Middle) The spheroidized condition, G. Carbide morphology: globular, inter- and intragranular. (Bottom) Pearlitic condition, P. Carbide morphology: lamellar, grain boundary.

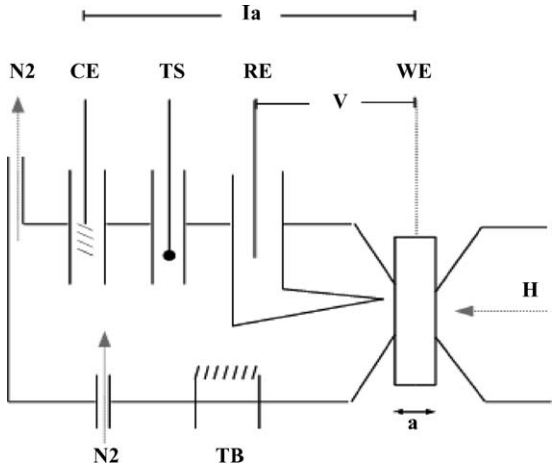

Fig. 5. Electrochemical cell for permeation tests. H detection compartment containing: a reference electrode (RE), the sample as work electrode (WE), the counter electrode (CE), a temperature sensor (TS), a termic circuit (TB), and the polarization voltage (V). Nitrogen (N_2) bubbling being maintained throughout the test.

are present during the former permeation test, and both influence the diffusion process of H through the metal. Then, a second permeation test is performed that allows to distinguish between the two kinds of traps. First, a previously hydrogenated sample is left in the reaction tube at an initial vacuum of 10^{-4} Torr for 1 h, followed by a final vacuum of 10^{-6} Torr for 2 h (both at 27 °C) to remove diffusible H. Then, heating rates of 2, 4, 6, and 8 K min^{-1} are applied, with a starting temperature of 308 up to 773 K. The H liberated for the sample is monitored with a pressure transductor subsequent to vacuum lost.

5. Connecting the model with the experimental data

A specific model describing the effects of reversible trapping on the relation between the permeation flux and test time, $P(t)$ versus t, was developed by Ferris and Turnbull [4]. Their treatment involve the elimination of $N_r(\partial n_r/\partial t)$ in Eq. (8) by replacing the left term of Eq. (9) into Eq. (8). This procedure reduces the problem to a non-linear parabolic equation in partial derivatives that requires a numerical solution. They propose a solution that satisfies the boundary conditions (10) and solve the equation by finite element. More simply, we directly solve the coupled system of differential equations (8) and (9) by employing subroutines from the library IMSL [3]. Within our picture, the parameters that affect most the shape of the permeation curves in presence of reversible trapping, and that describe the kinetics of hydrogen diffusion in steels, are λ, μ, ρ, and D_L. Next, we briefly describe the effects of these parameters on the normalized theoretical curves $P(t)/P_\infty$, $P_\infty = C_0 D_L/a$. Notice that $P(t)/P_\infty \equiv J/J_\infty$, being $J = I_a$ the anodic current shown in Fig. 5.

We verify that the shape of $P(t)/P_\infty$ does not depend on the λ alone, so that λ cannot be directly derived from $P(t)/P_\infty$. By assuming $\lambda > 10^2$, the equilibrium situation described by Oriani [6] is assumed, then Eq. (24) can be employed to calculate de binding energy ΔE. Our picture predicts that: (i) the effect of increasing λ/μ (maintaining $\lambda = \text{cte} > 10^2$) on $P(t)$ is equivalent to shifting the $P(t)$ of a lattice without traps to greater times, and (ii) the effect of increasing ρ to values larger than 10^{-3} is an increase of the slope of $P(t)$, which may be interpreted as a decrease of the trapping efficiency as time progresses, with the consequent effect of the hydrogen transport becoming less delayed, so reaching the steady state more quickly. The above parameters must be fitted altogether; after best fit is obtained the binding energy ΔE, the density of reversible traps N_r and the rate between capture and release probabilities k_r/p_r from the values of λ, μ and ρ are derived.

5.1. Details of the binding energy calculation from electrochemical permeation tests

As mentioned the experimental separation of reversible and irreversible trapping sites is made through sequential permeation tests. Irreversible traps are filled during the first test and do not have any influence on second ones, then the effects of the reversible trapping sites can be isolated.

In order to quantify the trapping parameters, an appropriate election of D_L is essential. In this sense, the best representation of D_L in the temperature range 40–80 °C for bcc iron is [7]: $D_L = 7.23 \times 10^{-4} \exp(-E_a/RT)\ \text{cm}^2\ \text{s}^{-1}$, where $E_a = 5.69$ kJ/mol. The binding energy ΔE is calculated from Eq. (24) related to λ, μ, ρ, C_0 and N_r (the density of reversible traps). Here, C_0 represents the H solubility in the material surface exposed to the H compartment of the electrochemical cell (Fig. 3). We use the IMSL subroutines [3] to solve the coupled differential equations (12)–(14), which relate experimental data to the model parameters. The fits are performed for the second permeation curves, by varying λ/μ and ρ simultaneously. The quotient λ/μ can be estimated from an expression for D_L deduced by Oriani [6]; in the situation of fast equilibrium between two populations, D_L can be expressed as a function of λ/μ as

$$\frac{\lambda}{\mu} = \frac{D_L}{D_{app}} - 1, \tag{25}$$

where D_{app} is calculated from the second permeations test shown in Fig. 5, following Appendix A procedure, by adopting D_L (35 °C) = $783 \times 10^{-5}\ \text{m}^2\ \text{s}^{-1}$ [7]. Assuming local equilibrium we calculate ΔE from Eq. (24),

$$\frac{k_r}{p_r} N_L = \frac{N_L}{C_0} \rho \left(\frac{\lambda}{\mu}\right) = \exp\left[-\frac{\Delta E}{RT}\right],$$

where $N_L = 5.2 \times 10^{23}\ \text{cm}^{-3}$ is the density of tetrahedral sites per unit cell for Fe–Ti–C alloys. The parameters ρ and λ/μ are in term obtained from the best fit. To determine their optimum values, we define intervals $(\lambda/\mu|_{min}; \lambda/\mu|_{max})$ and $(\rho_{min}; \rho_{max})$, and use them to setup a 2D 10 × 10 grid. The optimum value of $(\lambda/\mu; \rho)$ is the grid point that minimizes the mean square deviation between numerical and experimental permeation curves.

In order to calculate the binding energy from the vacuum desorption test the "differential thermal analysis" methodology adopted by Choo and Lee [5] (summarized in Appendix B) is employed. From the peaks (T_p) and the respective heating rates,

ϕ, a graph $\ln(\phi/T_p^2)$ versus T_p^{-1} is drawn; the binding energy is directly obtained from the slope of the straight line $\ln(\phi/T_p^2) \propto |\Delta E| T_p^{-1}$.

The density of reversible traps and the liberation percentage are obtained from $N_r = C_0/\rho$ and $p_r = \mu D_L/a^2$, respectively, once C_0 has been determined. Knowing the value of N_r, the capture probability is calculated through the expression $k_r = \lambda D_L/a^2 N_r$.

6. Results and discussion

The results of the thermal treatments to obtain the three-cementite morphologies are shown in Fig. 3. Optical microscopy reveals an equiaxed grain structure for the three carbides as shown in Table 1, so reducing the number of microstructural variables, which could influence the diffusion process. Fig. 2(a)–(c) reports the optical micrographies of the three morphologies (A, P and G) for the three plate cuts; the rolling direction is indicated. In sample G iron carbides are very characteristic, that is, spheroidized in the ferritic matrix, whereas and a preferential presence of the pearlite colonies at the grain boundaries is observed in sample P. In samples A, the precipitates are not revealed by OM. The transmission electron micrograph of Fig. 4 shows the typical carbide morphologies for each condition. In the case of the pearlitic microstructure, the cementite exhibits a fine lamellar morphology with lamellae typically around 100 nm thick and an interlamellar spacing of approximately 0.05 μm. The pearlite colonies are observed to be situated along the pro-eutectoid ferrite grain boundaries. The spheroidizing treatment modifies this morphology, producing globular carbides with diameters of approximately 0.6 μm, situated close to the grain boundaries. The aging treatment results in a homogeneous dispersion of very fine intergranular carbides, typically around 20 nm in diameter.

The current model for analyzing the diffusive behavior from permeation tests uses four parameters, D_{app}, N_r, p_r and k_r that describe the physical state of the medium, instead of the single parameter D_L of the more elemental theory. In addition, C_0 must be found indirectly and is therefore an extra parameter ($P_\infty = C_0 D_{app}/a$). Of these five unknowns, steady state experiments can at most determine C_0, D_{app}, N_r, and the ratio k_r/p_r. Besides, an analysis of the resulting data in terms of the unidirectional diffusion of hydrogen in the thin metallic sheet allows the determination of the three parameters that quantify the permeation behavior: permeability $P(t)$, apparent diffusivity D_{app}, and apparent solubility S_{app}. We calculate these parameters following the methodology described in Appendix A and the results are summarized in Table 2 for three successive permeation tests on each sample. Fig. 6 shows the experimental permeation curves for sample A together with the theoretical one that best fit the experimental data. It is seen that for times greater than 80 min the fitted and experimental profiles differ, while for $t < 80$ min the agreement is excellent. As shown in Appendix A, the permeability P_∞ is calculated from $P_\infty = aJ_\infty \propto ai_\infty$, being a is the sample thickness, J_∞ the H flux through an arbitrary surface, and i_∞ is the experimental anodic current (Fig. 5). In the steady state P_∞ is independent of traps, so that the 1st Fick law is valid, then $J_\infty = D_{app} C_0/a$, allowing the determination of $C_0 \equiv S_{app} = P_\infty/D_{app}$, the H solubility in the material surface exposed to the H compartment of the electrochemical cell (Fig. 3); D_{app} is determined before by following the procedure of A.1. Table 2 summarizes the results obtained for D_{app}, P_∞ and S_{app} for each carbide condition. The procedure is more accurate than the standard electrochemical method [8] based on time measures, because permeation times are affected by superficial effects such as oxide shells. Within our procedure only the initial part of $P(t)$ is used to perform the fit, as shown in Fig. 4 for morphology A, so that oxidation effects do not influence the determination of the kinetics parameters.

Table 1
Ferrite grain size of samples A, P and G for different sample sections

Sample	Cut surface	Grain size (μm)
A	S_{xy}	18.93 ± 0.14
	S_{yz}	19.20 ± 0.39
	S_{xz}	18.31 ± 0.21
G	S_{xy}	20.06 ± 0.03
	S_{yz}	18.94 ± 0.56
	S_{xz}	19.47 ± 0.17
P	S_{xy}	20.24 ± 0.21
	S_{yz}	19.84 ± 0.67
	S_{xz}	19.48 ± 0.51

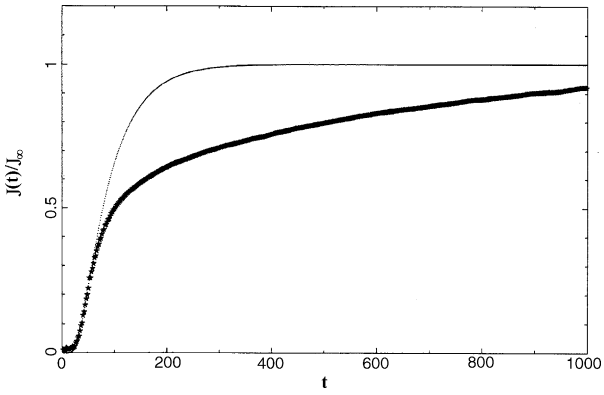

Fig. 6. Calculation of the permeation parameters: normalized experimental permeation curves together with the best fit for sample A as a function of time test.

Fig. 7 shows the permeation kinetics observed for each type of sample as a plot of $P(t)$ (normalized to P_∞ versus the time test). As reported in Table 2 the apparent hydrogen diffusivity in the pearlitic material is significantly higher than for the other two studied microstructures. It could reflect the effectiveness of the semi-continuous pearlite ferrite interphase at the pro-eutectoid ferrite grain boundaries, characteristic of this material, as a preferential hydrogen diffusion path. The apparent solubility values obtained for the three conditions reveal a higher solubility for the aged structure than for the other two conditions, although the relative differences in this parameter do not reflect the large difference in S_V (specific interphase area) qualitatively calculated by Bott et al. [1]. This confirms that the cementite pro-eutectoid ferrite interphase is relatively inefficient as a

Table 2
Apparent diffusion coefficient (D_{app}), apparent solubility (S_{app}) and permeability at the steady state (P_∞) obtained from electrochemical permeations tests on samples A, G and P at 27 °C

Sample	Permeability	D_{app} ($\times 10^{-10}$ m^2 s^{-1})	P_∞ ($\times 10^{-10}$ mol H/mm^2 s)	S_{app} (mol H/m^3)	S_V ($\times 10^{-6}$ mol H/m^3) [6]
A	1st	2.19 ± 0.11	0.65 ± 0.02	0.49 ± 0.01	171.7
	2nd	2.62 ± 0.15	0.14 ± 0.05	0.15 ± 0.03	171.7
G	1st	3.47 ± 0.11	1.07 ± 0.02	0.29 ± 0.02	2.3
	2nd	3.94 ± 0.25	0.65 ± 0.04	0.16 ± 0.01	2.3
	3rd	4.18 ± 0.18	–	–	2.3
P	1st	6.43 ± 0.40	1.16 ± 0.04	0.17 ± 0.02	4.7
	2nd	7.78 ± 0.39	0.85 ± 0.03	0.10 ± 0.02	4.7
	3rd	8.01 ± 0.32	–	–	4.7

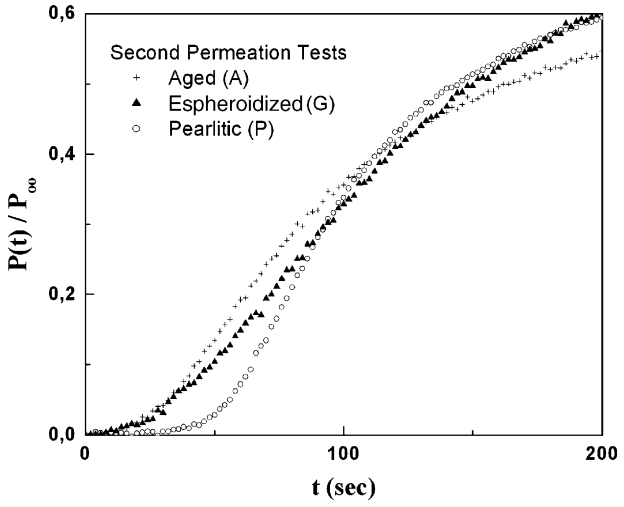

Fig. 7. Normalized hydrogen permeability curves. Hydrogen permeability in low-carbon steel normalized to the steady-state asymptote as a function of permeation time at 300 K for the three carbide morphologies: P, pearlitic; G, globular; A, age.

hydrogen-trapping site at room temperature as reported by Bott et al. [1].

The best fitted value for each set of experimental data are $\lambda/\mu = 29$, $\rho = 7.5 \times 10^{-4}$ for the *aged* (A) sample, $\lambda/\mu = 20$, $\rho = 1.0 \times 10^{-3}$ for the *globular* (G) sample and $\lambda/\mu = 10.5$, $\rho = 5.0 \times 10^{-3}$ for the *pearlitic* P sample. Hydrogen binding energies, ΔE, are reported in Table 3, as well as the density of reversible traps together with the H capture and release probabilities. The reversibility criterion is based on the quotient $\Delta E/k_B T$. From Table 3, the calculated depth of the potential well associated with the trapping sites results $\Delta E = 4.5$ kJ/mol H, which is lower than the activation energy, $E_a = 5.69$ kJ/mol H, of the perfect lattice. So that, the calculated activation energy of the traps, $E_{aT} = \Delta E + E_a$ (assuming $E' = 0$), amounts to $E_{aT} = 10$ kJ/mol H.

Table 3
Calculated parameters describing reversible trapping from electrochemical tests

Sample (300 K)	ΔE (kJ/mol H)	N_r ($\times 10^{-19}$ sites cm^{-3})	k_r/p_r ($\times 10^{19}$ cm^{-3})
A	4.70 ± 0.89	12.00 ± 1.04	2.39 ± 0.21
G	4.55 ± 1.01	9.94 ± 0.86	2.01 ± 0.18
P	4.68 ± 0.94	4.30 ± 0.96	2.17 ± 0.15

As reported in Table 3 the morphology that possesses the greater density of reversible trapping sites is the aged one. This result is consistent with the apparent diffusivity measured within the second permeations, namely, lower than the ones for the other two morphologies. The effect of irreversible traps can be seen from the results of the first permeations when compared to the second ones. The values of D_{app} in the former are lower than in the latter due to both kinds of traps (reversible and irreversible), which are active during the diffusion process. Consistently, the apparent solubility of hydrogen, S_{app}, appears to be, i.e., it would increase with the density of traps. The effect of the oxide shell, which modifies the diffusion kinetics, can be minimized by palladium deposition (the electrochemical boundary conditions are so quickly satisfied), or by sputtering in ultra high vacuum and then spraying with Ar. This technique prevents the formation of oxide shells on the material surface.

Sample A, when subjected to effusion tests, shows a single peak at a heating rate $\phi = 2$ K min^{-1}, Fig. 8. Perhaps, characteristic peaks for this sample moved to temperatures higher than 600 K. Due to the metastable nature of the cementite, it may occur that the microstructural evolution, due to the wide range of considered temperatures, disables the distinction of peaks. The unstable evolution of the A microstructure during the ther-

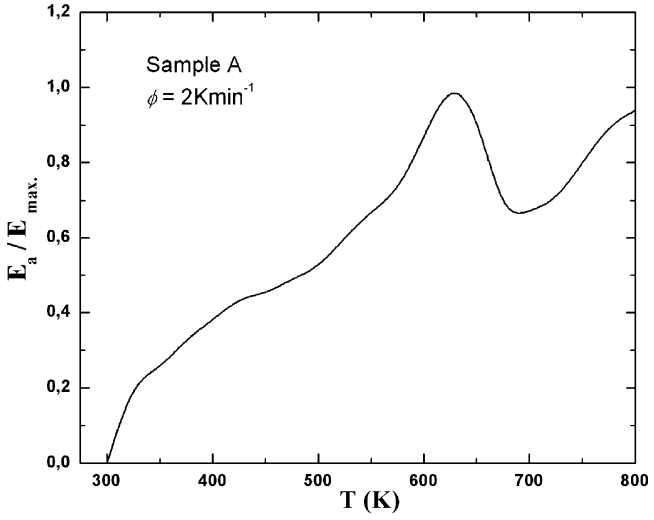

Fig. 8. Thermal effusion curve as a function of the temperature, renormalized to the maximum effusion value (E_{max}) for sample A.

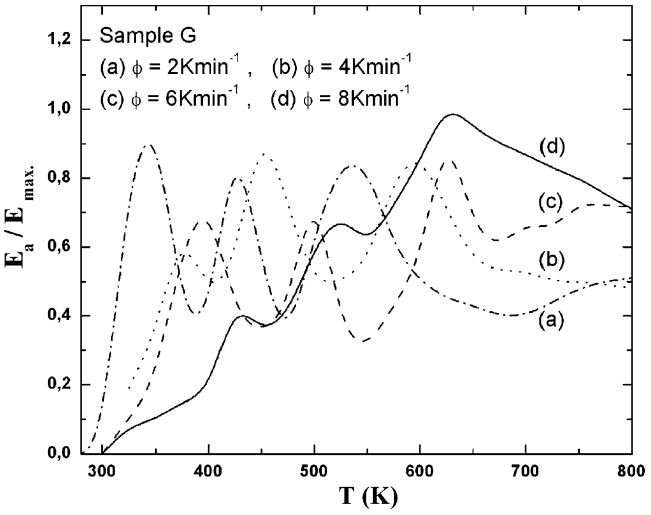

Fig. 9. Thermal effusion curve as a function of the temperature, renormalized to the maximum effusion value (E_{max}) for sample G.

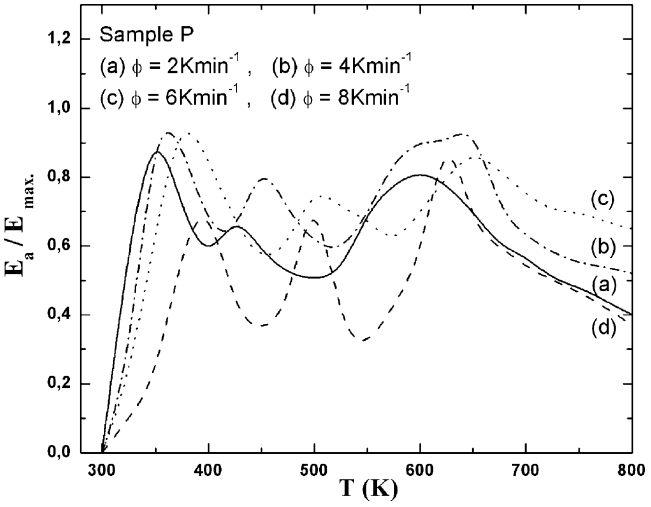

Fig. 10. Thermal effusion curve as a function of the temperature, renormalized to the maximum effusion value (E_{max}) for sample P.

mal analysis did not allow us the determination of the binding energy. For the samples G and P, three peaks appear in the effusion curves, as shown in Figs. 9 and 10. Values of ΔE found for each peak are reported in Table 4 as calculated from the slopes of the straight lines of Figs. 11 and 12.

H originating in the ferrite/cementite interphase may be held responsible for the first peak observed for samples G and P, reinforcing the concept [1] that the spheroidized cementite and the one present in pearlite layers is crystallographically incoherent with the ferritic matrix. A second peak is observed in samples G and P, which reveals the existence of some trap common to

Table 4
Binding energies calculated from efusion tests for samples G and P

Sample (300 K)	ΔE_1 (kJ/mol H)	ΔE_2 (kJ/mol H)	ΔE_3 (kJ/mol H)
G	13.10 ± 1.59	23.80 ± 3.57	40.10 ± 8.80
P	12.90 ± 3.40	25.40 ± 3.07	50.31 ± 4.58

ΔE_i, i = 1–3 indicates corresponding T_p.

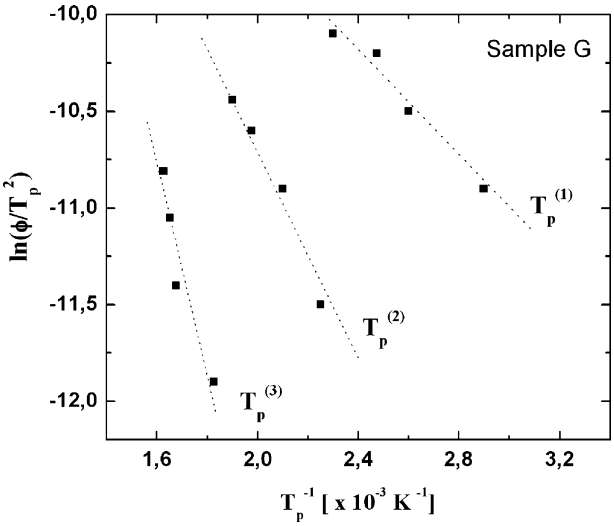

Fig. 11. Temperatures T_p (j) of j = 1st, 2nd and 3rd peak as a function of the heating rate for sample G.

both, due to the close values of ΔE. The average ΔE value for these samples, 24 kJ/mol H, makes us believe that the hydrogen leaving the samples may originate from the dislocations, and is consistent with the results obtained by Hong and Lee for samples of pure polycrystalline iron $\Delta E \approx 26.8$ kJ/mol H [9]. It is emphasized that the nature of the aged ferrite interphase, which possesses fine carbides of crystallographic coherence with the ferritic matrix, is probably able to trap H in a more complex way. Finally, the third effusion peak, Figs. 7 and 8, at values of $\Delta E \approx -(40, 50)$ kJ/mol H are deep traps. The origin of this peak may be very diverse, for peaks with $\Delta E \approx -50$ kJ/mol H the microstructural species responsible for the trapping cannot be known with certainly. Iino [10] has studied a steel similar to the one employed in this work, obtaining binding energies of approximately −84 kJ/mol H. He identified this peak as the desorption of H from in magnesium sulfide (MnS) present in the alloy, assumption based on TEM observation. Therefore, this precipitate might at first be held responsible for the third peak

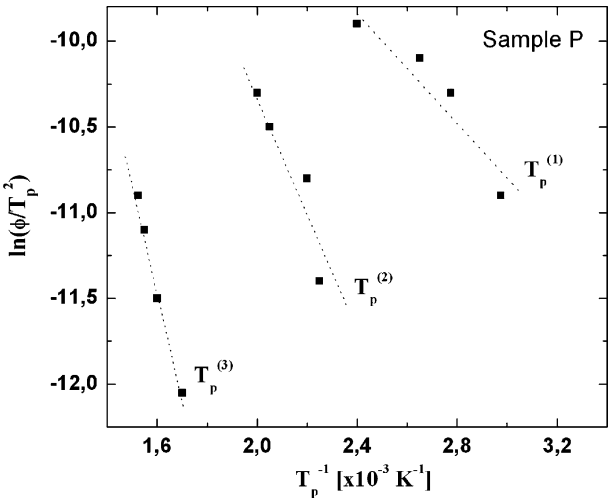

Fig. 12. Temperatures T_p (j) of j = 1st, 2nd and 3rd peak as a function of the heating rate for sample P.

is our case as well. Although the presence of alumina (Al_2O_3) is revealed by its physical aspect, it is much more probable that the H is accumulated in the inclusions of MnS in an irreversible way, since these present a larger free volume.

Luppo and Ovejero-García [11] using the electrochemical permeation method (electrochemical and gas charging), mechanical tests, and hydrogen microprint technique, obtain similar values of ΔE with different microstructural specimens in low-carbon steels. These authors state that in the case of steels this fact is due mainly to dislocations. In contrast Oriani [7] has assumed that in annealed steels the main H trapping sites are the interphases between precipitates, and Ono and Meshi [12] has attributed energies of the order of 49 kJ/mol H to grain boundaries. Cleary, the matter in under debate, and we prefer to leave the question of the microstructural species responsible for the third peak open.

7. Conclusions

Electrochemical techniques are employed to study the nature of three morphologies of the cementite as trapping sites at 300 K, combined with a reformulation of Fick's equations considering that the permeation of hydrogen atoms diffusing through the substrate is delayed by traps. The results, when compared to those qualitatively obtained by Bott et al. [1], show that hydrogen is inefficiently (reversibly) trapped at $T = 300$ K for the three studied conditions. Changes in the carbide morphology of low-carbon steels do significantly alter the permeability, the diffusion constant, and the apparent solubility of hydrogen, as well as the density of reversible traps. However, the morphology of the carbide seems to have less influence on the binding energy.

The kinetics of H permeation in low-carbon steels is considerably altered by the morphology of the cementite. The presence of fine cementite in the aged ferrite increases solubility and reduces H diffusivity in the studied steel whereas, when arranged in layers as in the pearlite, it increases the diffusion coefficient and reduces solubility. On the other hand, the spheroidized structure presents intermediate values in comparison with the previous two. The cementite reveals itself as a deep H trap for certain temperatures. Binding energies in the interval of 10–50 kJ/mol H are obtained, corresponding to the weak and strong interaction of H with the trapping sites. Combining H vacuum effusion techniques with electrochemical permeation tests allows performing an exhaustive analysis on the kind of traps, reversible and irreversible, present in a sample. The effusion technique shows the presence of several kinds of traps in the sample, while relevant parameters of a single species are obtained from the electrochemical tests of the second permeations. In the curves of the first permeations, both kinds of traps are present but their separation is not possible from the theoretical point of view. For this reason, effusion techniques are applied. Both techniques are complementary, since it is possible to obtain the relevant diffusion parameters, such as the coefficient of apparent diffusion, the apparent solubility and the permeation in the stationary state as well as the binding energies of several microstructural species that are present in the sample and act as trapping sites of H.

Acknowledgements

The authors would like to thank Dr. P. Bruzzoni, Dr. J. Fernandez and Dr. R.C. Pasianot for valuable discussions on the present work. This work has been partially supported by Universidade Estadual de Vitória, ES, Brazil.

Appendix A. Diffusion coefficient calculation

The deviation of the permeation curves related to the ideal situation (Fe_α) can be employed to determine the apparent diffusivity in presence of traps in the context of local equilibrium described by Oriani [6]. In this case, Fick's second law, which describes the behavior of hydrogen transport in steels by replacing D_L by D_{app} includes the effect of trapping. The solution of the modified Fick's second equation is known and the methodology employed to determine D_{app} is described as follows. With the purpose of evaluating the electrochemical results, it is necessary to obtain an expression of the anodic current $I_a(t)$. From Fick's first law, $J(x, t) = -D_{app}\partial C(x, t)/\partial x$ and $J(x = a, t)$ related with $I_a(x = a, t)$, being a the sample thickness, through.

$$I_a(t)|_{x=a} = -qfD_{app}\left[\frac{\partial C(x,t)}{\partial x}\right]_{x=a}, \tag{A.1}$$

where q is the sample area exposed to permeation and f is the Faraday constant. One possible solution of Eq. (1) that satisfies the boundary conditions (10) experimentally established is

$$C(x,t) = C_0 - C_0\frac{x}{a} + \frac{2}{\pi}\sum_{n=1}^{\infty}\frac{C_0}{n}\sin\left(\frac{n\pi x}{a}\right) \times \exp\left(-\frac{D_{app}n^2\pi^2}{a^2}\right). \tag{A.2}$$

Substituting Eq. (A.2) in (A.1), finally, the expression for the anodic current $I_a(t)$ is,

$$I_a(t)|_{x=a} = i_\infty\left(1 - 2\sum_{n=1}^{\infty}(-1)^n\exp\left(-\frac{D_{app}n^2\pi^2}{a^2}t\right)\right), \tag{A.3}$$

where $i_\infty = D_{app}C_0qf/a$ is the value of the anodic current at the steady state. If $P_1 = i_\infty$ and $P_2 = (a^2/\pi^2)D_{app}$ Eq. (A.3) take the form:

$$I_a(t)|_{x=a} = P_1\left(1 - 2\sum_{n=1}^{\infty}(-1)^n\exp\left(\frac{n^2}{P_2}t\right)\right). \tag{A.4}$$

Varying the parameters P_1 and P_2 allows the fit of the theoretical curve to the experimental data. The effect on the permeation curves of the P_2 parameter is to modify the slope of the transitory of the normalized anodic current. Known the value of P_2 the apparent diffusivity is determined. The effect of increased P_2 is to decrease the slope of the transitory. It may be interpreted as an augmentation of the trapping efficiency as time progresses, with the consequence of hydrogen transport becoming more delayed and the steady state reaching more slowly.

Physically, this is reflected by the diminution of the apparent diffusivity when compared to the diffusivity of the perfect lattice, whereas a decrease of P_2 has the opposite effect. Then, the variation of P_2 is an indirect measure of D_{app}.

Appendix B. Binding energy calculation from effusion tests

The study of the binding energy of H with microstructural species (or traps) in metallic materials is based on kinetics and diffusion in the solid state. Different mathematical models applied to the desorption technique (thermal effusion in a vacuum) are found in literature. Next, a model is presented, which is developed by Lee et al. [5], who start from the principle that H solubilized by a metal (H) is trapped by an X trap, according to reaction:

$$\underline{\mathrm{H}} + \mathrm{X} \Leftrightarrow \mathrm{H_X}. \tag{B.1}$$

Assuming that the X trap acts as a potential well, where H imprisoned by this trap (H_X) is found in S_X, shown in Eq. (B.1), the velocity of H escaping from a trap is given by

$$\frac{\partial \mathrm{X_T}}{\partial t} = A(1 - \mathrm{X_T}) \exp\left(-\frac{E_\mathrm{L}}{RT}\right), \tag{B.2}$$

where $X_T = (C_{(x,0)} - C_{(x,t)})/C_{(x,0)}$, being $\partial X_T/\partial t$ is the escaping velocity of H from the trap or effusion velocity of H. $C_{(x,0)}$ is the initial concentration of H in the trap and $C_{(x,t)}$ is the concentration of H in the trap for an arbitrary $t \neq 0$. A is the constant of the reaction (B.1), R the constant of ideal gases and T is the absolute temperature. The exponential term in (B.2) is the probability of H of leaving a trap ($E > E_a$). Therefore, when subjecting a metallic specimen containing a certain quantity of H in solid solution to a thermal effusion test in a vacuum, it is expected to observe several peaks of H escaping, which are related to the traps present in the specimen. If Eq. (B.2) is differentiating in relation to time and equating the result to zero, the maximum effusion rate of H is obtained, as a function of temperature T. Applying Neperian logarithm (ln) to the temporal derivative (B.2) related to $1/T_p$, where T_p is the temperature at which a peak in the effusion curve occurs, the following relation is obtained:

$$\frac{\ln(\phi/T_\mathrm{p}^2)}{1/T_\mathrm{p}} = -\frac{|\Delta E|}{R}. \tag{B.3}$$

where ϕ is the heating rate. Eq. (B.3) allows determining the binding energy of H with the three morphologies of the cementite. For this purpose, it is sufficient to obtain the T_p from the effusion curves and their corresponding heating rate ϕ. As the heating rate imposed over each specimen is varied, T_p is modified. Finally, drawing a graph $\ln(\phi/T_p^2)$ versus $1/T_p$, the binding energy ΔE is obtained from the slope of the resulting straight line.

References

[1] A.H. Bott, D.S. Dos Santos y, P.E.V. de Miranda, J. Mater. Sci. Lett. 12 (1993) 390–393.
[2] A. McNabb, P.K. Foster, Trans. Metall. Soc. AIME 227 (1963) 618.
[3] G. Sewell, IMSL Software for Differential Equations in One Space Variable, IMSL Technical Report Series 8202, June 1982.
[4] D.H. Ferris, A. Turnbull, NPL Report DMA (A) (1988) 154.
[5] W.Y. Choo, J.Y. Lee, Metall. Trans. A 13 (1982) 135–140.
[6] R.A. Oriani, Acta Metall. 18 (1970) 147.
[7] K. Kiuchi, R.B. Mc Lellan, Acta Metall. 31 (1983) 961.
[8] N. Boes, H. Zuchner, J. Less-Common Met. 49 (1976) 273.
[9] G.W. Hong, J.Y. Lee, Acta Metall. 32 (10) (1984) 1581–1589.
[10] M. Iino, Metall. Trans. A 18 (1987) 1559–1564.
[11] M.I. Luppo, J. Ovejero-García, Corr. Sci. 32 (1991) 1125–1136.
[12] K. Ono, M. Meshi, Acta Metall. 40 (1992) 1357–1364.